Available online www.jsaer.com

***Journal of Scientific and Engineering Research*, 2024, 11(9):31-53**

Research Article

ISSN: 2394-2630
CODEN(USA): JSERBR

Design and Finite Element Analysis of Coronary Bifurcation Stents

Ujwala Thejeswini[1], Rajeev Nair[2]

[1,2]Department of Mechanical Engineering, Wichita State University, Wichita, Kansas, USA

Abstract: Atherosclerosis is the leading cause of death in the world. Continuous and ongoing research on the treatment for atherosclerosis are being developed. The most common advanced Atherosclerosis treatment or procedures is the use of stents which provides scaffolding to the blocked artery and treat the diseased region of the arteries by the drugs coated on them.Numerous stents are being developed to treat the bifurcation lesions to reduce its recurrences, stents ranging from bare metallic stents, dedicated stents with a carina or easy access to side branches, drug eluding stents and bio degradable stents. Due to the increased complexity of bifurcation lesions, the stent design by itself should be coupled with an effective stenting procedure for successful treatment. The stenting techniques cause distortion in the region where the arteries branch out which results is complications during and after the stenting procedure. This study is aimed towards finding the best design approach for bifurcation stents, to compare the studied designs and to come up with the best suitable design for diseased bifurcated arteries which includes design of a new stent which is a Sinusoidal Helix, i.e. a sinusoidal wave running helically. The idea behind this is to minimize the jailing of the main stent and the side branch stent, hence reducing the distortion. Finite Element Analysis is performed on these designs to compare the displacement, Von Mises Stresses, Factor of Safety using materials such as 316L SS, Cobalt chromium alloy and Magnesium alloy.

Keywords: Coronary Bifurcation Stents, Finite Element Analysis, Helical Model, Parametric Design, Peak to Peak, Peak to Valley

1. Introduction

A is the major cause of morbidity and mortality representing up to 50% deaths in the western world. It is a condition where plaques restrict the flow of blood in arteries. The coronary heart disease is the most common disease affecting a large percentage of the world's population [1-3]. In America alone, about 8 million of them have heart attacks due to atherosclerosis and a third of the deaths of people older than 35 is due to coronary heart disease.

Coronary Bifurcations which are the regions where the coronary arteries branch into smaller vessels that carry blood to the heart in the human body are prone to atherosclerosis. Atherosclerosis is a condition where the arteries get hardened and narrowed due to the plaque accumulation caused by the combination of calcium, fat, and other substances due to the presence of cholesterol in the blood stream. These cholesterol plaques can behave in different ways [4, 5]. They can stay inside the artery wall, may stop growing, or may even grow into the wall, out of the path of blood. They can rupture suddenly which causes blood clots in the artery. If the clogged artery supplies blood to the heart, it results in a heart attack. The plaques that grow in a slow, controlled way may severely block arteries, sometimes without causing any symptoms. The diseased arteries are treated

through surgical or interventional procedures to prevent additional arterial plaque accumulation among which Stenting is the most common procedure used.

Stent placement is called Percutaneous Coronary Intervention (PCI) which is a non-surgical procedure of inserting a small meshed tube like structure called a stent inside the artery, which may contain medication to treat the diseased artery locally and to maintain adequate blood flow. This tubular structure that is left inside the lumen of a diseased artery to relieve an obstruction due to plaques [6-9]. Commonly, stents are inserted in a non-expanded form and are then expanded autonomously (or with the aid of a second device in situ). A typical method of expansion occurs using a catheter mounted angioplasty balloon which is inflated within the stenosed vessel or body passage way to shear and disrupt the obstructions associated with the wall components of the vessel and to obtain an enlarged lumen. A catheter is used through the artery of the leg to reach the heart, and a stent is put in place and expanded using balloon expansion method or using self-expanding stents.

Stents can be classified based on the deployment method as self-expandable stents and balloon expandable stents. The classification effects the way the stent is manufactured, the balloon expandable stents are manufactured in the crimped state and expanded to the vessel by fitting it over a deflated balloon and inflating it when the stent reaches the diseased part in the artery. The stent gets plastically deformed in this method. The Self expandable stents are manufactured at the required expanded diameter or slightly larger than that, and then crimped to a smaller diameter to be able to be deployed to the diseased region of the artery. Once the self-expandable stent reaches the intended region, the sheath holding the crimped stent is withdrawn and the stent expands to the manufactured diameter [7-11]. Bifurcated arteries are a common site for the buildup of atherosclerotic plaque due to the differences in blood flow, shear stress and turbulence at the site of the bifurcation. The occurrence of bifurcation stenosis in coronary arteries is reported to be between 15% to 20% of all interferences and is complex and challenging for percutaneous intervention. Numerous stents are being developed to treat the bifurcation lesions to reduce its recurrences, stents ranging from bare metallic stents, dedicated stents with a carina or easy access to side branches, drug eluding stents and bio degradable stents. Due to the increased complexity of bifurcation lesions, the stent design by itself should be coupled with an effective stenting procedure for successful treatment [12-18]. There are several stenting procedures that are used to implant bifurcation stents: Crush Techniques, Culotte Techniques, Double-Kissing Techniques and T-Stenting Procedures. We observe that there is a jailing effect of stents in the bifurcated area causing deformations in the stent structure or there are areas where the stent does not reach. This research study is based on designing an effective stent structure which results in reduced deformations in bifurcation stents while maintaining a good coverage of the diseased artery [19-23]. The currently used stenting techniques cause distortion in the region where the arteries branch out (figure 1).

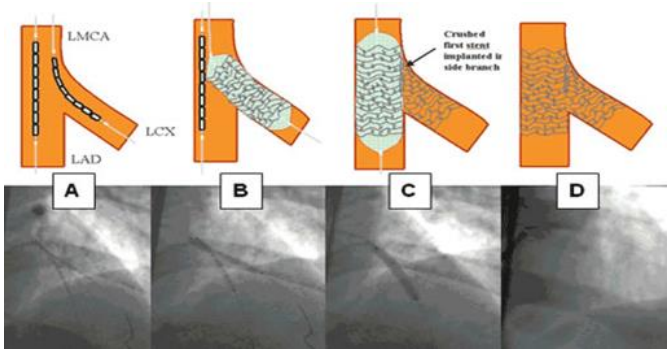

Figure 1: *Jailing effect [5]*

Our goals in this study is to to find the best design approach for bifurcation stents, and compare the studied designs and to come up with the best suitable design for diseased bifurcated arteries. Some of the current stent constructions are given in figure 2 below.

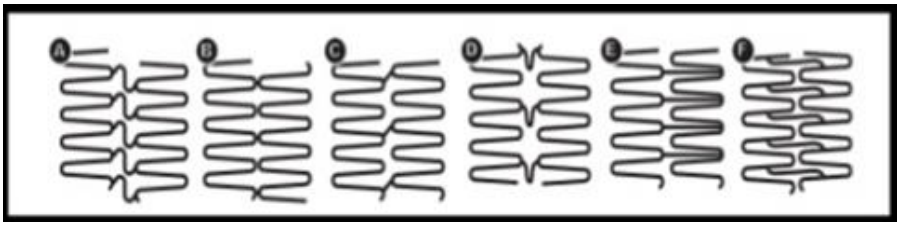

Figure 2: *Typical stent constructions: (A) Closed cell, peak-peak, flex connector (B) Open cell, peak-peak, nonflex connector (C) Open cell, peak-peak, nonflex connector (D) Open cell, peak-peak, flex connector (E) Open cell, peak-valley, nonflex connector (F) Open cell, mid-strut, nonflex connector [6]*

The new design objective is to design a stent which is a Sinusoidal Helix (figure 3), i.e. a sinusoidal wave running helically. The idea behind this is to minimize the jailing of the main stent and the side branch stent, hence reducing the distortion.

Figure 3: *Helical Design*

2. Design And Methods

The design process begins with understanding the requirements. The stent structure should have higher flexibility to be able to accommodate bifurcations in tortuous vessels require particularly conformable and flexible stents and good radial strength to prevent recoiling of the stent. And the geometrical basis is obtained from identifying the arterial diameters. The coronary tree is an object of fractal geometry governed by Murray's law [24]: The relation of the diameters between the Proximal Main Vessel (PMV) and its two (or more) distal branches is: PMV = (DMV + SB) * 0.67. Based on pathological, angiographical, intravascular ultrasound and computed tomography data coronary atherosclerosis appears to be more prevalent in the left coronary arterial system compared to the right (figure 4).

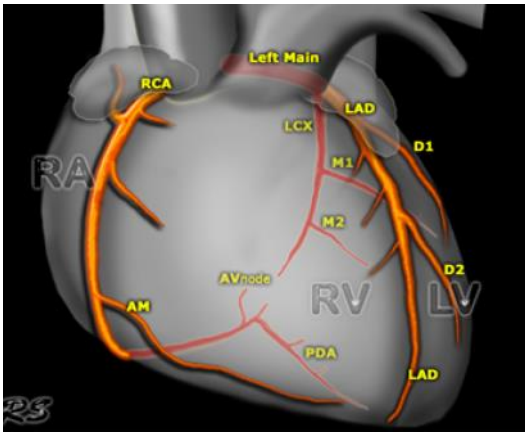

Figure 4: *Illustration of the Human Heart showing the right and left arteries [9]*

An analysis of the natural distribution of bifurcation angles by Multi-Detector Computed Tomography (MDCT) revealed average values of 80 +/- 27 degrees (LAD/LCX), 46 +/- 19 degrees (LAD/D1), 48 +/- 24 degrees (LCX/OM1), and 53 +/- 27 degrees (PDA/Rpld), respectively (figure 5).

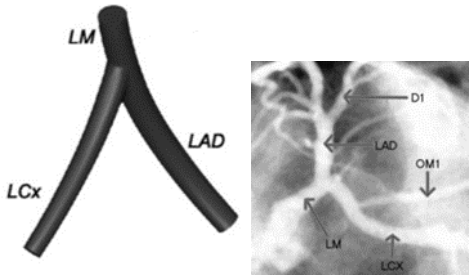

Figure 5: *Classification of Coronary Artery Bifurcation Lesions and Treatments.*

Where LAD stands for left anterior descending coronary artery, LCX stands for left circumflex coronary artery, LM stands for left main coronary artery, PDA stands for posterior descendent artery, OM1 stands for first obtuse marginal and RPLD stands for Ramus posterolateralis dexter which is the posterolateral branch [24-27]. Hence in general, the mean diameters of LMCA, LAD and LCX were tabulated as shown in table 1.

Table 1: Mean Diameters of LMCA, LAD and LCX

Artery Name	LMCA	LAD	LCX
Diameter (mm)	4.63	3.42	3.12

The mean diameter in males for LMCA is 4.86+/- 0.77mm, proximal LAD is 3.6+/- 0.58mm and proximal LCX is 3.26+/-0.65mm, while the mean diameter in females for LMCA is 4.5+/-0.73mm, proximal LAD is 3.31+/-0.46 and proximal LCX is 3.03+/-0.39mm. The diameter of the stent designed for LMCA in the current study is 4.5mm. The two studied models are industry standard stent design models [28]. The first model that was designed is the Abott Xience Xpedition-like stent- peak to valley structure as shown in figure 6.

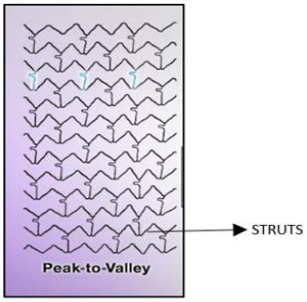

Figure 6: *Peak to Valley Design [1]*

The second model is the design of Bard LifeStar-like stent- peak to peak structure as shown in figure 7.

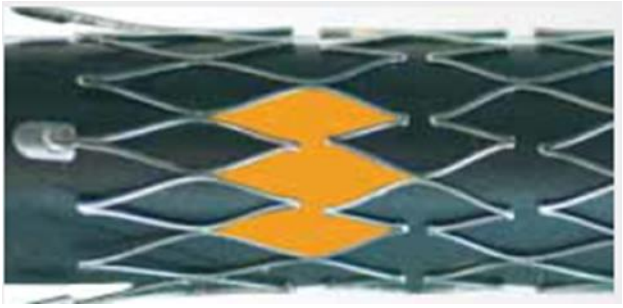

Figure 7: *Peak to Peak Design [13]*

Design Study of Model 1

The current stent model is Xience-like model and has a carina to aid in proper positioning of the side-branch stent. This prevents the fracture of stent structure during the stenting procedure, which has the potential to cause severe complications. This may result in restenosis or in-stent thrombosis. The presence of the carina makes it easy to predict the behavior of the stent [29]. The strut rings control the radial stiffness of the device. This design allows for strut rings to be closely packed along the length of the stent, resulting in an increased resistance to radial loading (figure 8).

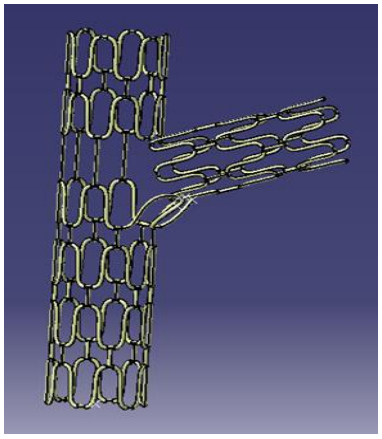

Figure 8: *Peak to Peak CATIA model*

Design Process

The stent design is parameterized on all struts and bridges except the distorted strut and the main branch is designed with a carina which makes way for a side branch during stenting procedure. The model is designed using generative shape design and solid modelling and the side branch is in contact with the main branch at the distorted strut area at four contact points.

Design Study of Model 2

The second model, which is a Bard LifeStar-like stent also has a carina for side branch access. In this model, the struts and bridges are connected peaks to valleys in struts. This design gives room for increased flexibility due to longer connectors being able to align better with the bends in the artery.

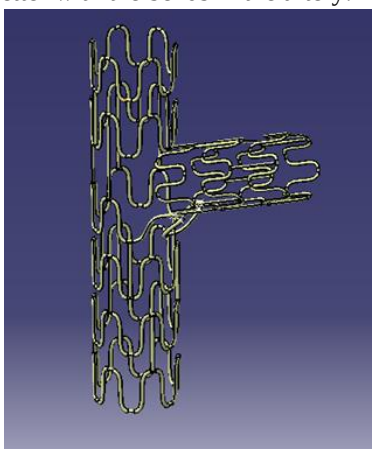

Figure 9: *Peak to Valley CATIA model*

Design process

The expanded stent model is modeled in generative shape modeling. This is parameterized and is dimensionally well controlled. The transition region where the expanded stent of the side branch overlaps on the main branch is modeled by dis-joining the transition strut surfaces and modeling the distortion that the main stent experiences due to the side branch overlap. To model the distorted surfaces, splines are used with tangency to the non-

distorted surfaces in the transition strut so that a continuous sweep can be generated without any sharp bends or edges. The surfaces are re-joined to obtain a complete strut containing distortion. The continuous struts which are closed surfaces are now converted to a solid in Part Body Design. This is done to be able to clean the model in the end and to extract the surfaces and join them to be able to use for FEA (finite element analysis). The position of the side branch is determined and a similar model approach is followed. The struts and bridges solids are joined using Boolean operations. The surfaces of the entire main branch are extracted and joined. The surfaces of the entire side branch are extracted and joined. Four contact points are created in the distorted region which defines the contact region between the two branches and does not allow the surfaces of the two branches to move one into another.

3. Parametric Modeling

CAD parametric modeling is to create 3D models that are complex yet flexible enough to allow changes to be made easily, keeping the integrity of the model intact. This modeling approach helps in adding, editing and deforming parts in the model while processing the design details. Surface modeling in CAD updates the co-ordinates of points, equations of curves and surfaces, as the model is created and modified on the screen. In parametric modeling, there are three methods by which a surface is created: By interpolation of points, by interpolation of curves, and by applying offset, revolve, translation and similar set of commands to the curves.

The modeling functions in the CAD program can move the shape characteristics. Examples of few functions are the sweeping and multi-sections functions. To define the surface profiles, the engineer adds geometric constraints and dimensions instead of specifying the shape. The geometric constraints relate the shape elements (perpendicularity, tangency, parallelism, midpoint etc.) and the program will generate the shape with respect to the dimensions specified. The sweeping function creates surfaces by translating or revolving profiles. Therefore, by changing the geometric constraints or the dimensions, the profile changes which also changes the surface. This design approach is called parametric modeling as various surfaces are created by changing their parameters. The fundamental problem with a pure parametric modeling approach as pointed out by David Weisberg, editor of the Engineering Automation Report, is that as the geometry is created, it is dependent upon the earlier generated geometry which is described as a parent/child relationship, which could be many levels deep. If a parent level element is deleted or changed, it can have unexpected errors/effects on child-level elements. Sometimes, the whole model needs to be recreated.

Parametric modeling and adaptations

Before starting a parametric model, it is ideal to always use formulae to parameterize the model, as it keeps the whole model linked, preventing gaps and errors. Also using tangency in splines to avoid sharp bends and connexity errors (the errors that occur when joining elements whose joining parameters don't agree) is prefered. Having a clear, detailed plan for the design intent, i.e., what is expected from the model in terms of model behavior towards parameterization and keeping the structure active using the datum feature in CATIA while joining surfaces (to be able to add more surfaces to the main surface) is critical. The create datum is deactivated, and there are no links to other entities in the model. To edit parts of a continuous surface, it is desired to disconnect the surfaces from the model by de-activating the datum feature and disassemble the desired surfaces. While joining cylindrical surfaces that are perpendicular to each other, the diameter of one element should be small enough compared to the other element to be able to eliminate free edges. The merging distance which is the tolerance by which the elements should be one, could be altered to manage very small dimensions. This ensures that there is no meshing failure. Initially when the model was built entirely using surfaces, the model failed to join as a complete model and threw connexity errors at regions where the bridges met the struts. This is due to merging of three surfaces. This error was eliminated by using sketches and pad option in solid part design. The resulting hybrid design was joined to form one single entity by converting all the closed surfaces into solids and added to form one body using Boolean operation. The model failed to mesh as the regions of bridge and strut connection after the Boolean operations left very small free edges or gaps. This was eliminated by reducing the bridge diameter by 0.002 mm which resulted in good merging of the solids.

4. Fe Modeling

As the cross-section of the stent structure is circular, the external surfaces are extracted and modeled. The stent model is meshed using 2-D quad elements with an element size of 0.05 mm. The Sag in the elements are controlled by 0.009 mm which results in better modeling of the circular cross-section. (The sag is a parameter that controls deviation between two elements). An FE quality check is performed and the bad elements are edited to obtain good meshing quality. The desired material is applied to the model. The materials used are; 316L stainless steel annealed (table 2), which is an extra-low carbon version of the 316-steel alloy and has excellent corrosion resistance; and, cobalt chromium alloy- Co-20Cr-15W-10Ni, which is a more ductile alloy and is used in cardiovascular applications. (this material has excellent in-vivo resistance to corrosion (table 3)), and magnesium alloy WE43: extruded, which is one of the latest advanced biomaterial known for the manufacture of biodegradable stents (table 4).

Table 2: Physical properties of 316L Stainless Steel [4]

Material	Composition, wt%	Elastic modulus, GPa (Msi)	Tensile strength σ_y, MPa (ksi)	Ultimate tensile strength σ_{ult}, MPa (ksi)	Elongation, %
316L stainless steel, annealed	17Cr, 12Ni, 2.5 Mo, <0.03C, balance Fe[a]	193[b] (28)	260[a] (38)	550[a] (80)	50[a]

The cobalt chrome alloy which is stronger than stainless steel gives us the opportunity of manufacturing thinner struts with the same radial strength. Also, this alloy is denser than stainless steel and hence is more radiopaque which helps monitoring the stent during the placement procedure.

Table 3: Physical properties of Co-20Cr-15W-10Ni [7]

Property	Minimum to maximum value	
	Metric	US
Compressive strength	283–313 Mpa	41–45.4 ksi
Tensile strength	773–1180 MPa	112–172 ksi
Bulk modulus	178–188 Gpa	25.9–27.2 10^6 psi
Young's modulus	222–240 GPa	32.1–34.9 10^6 psi
Shear modulus	86.9–87 Gpa	12.6 10^6 psi
Flexural strength (modulus of rupture)	310–427 Mpa	45–61.9 ksi
Elongation	23.6–49.2 %	23.6–49.2 %
Hardness - Vickers	220–300 HV	220–300 HV
Rockwell C Hardness	19.2–51.8	19.2–51.8
Mechanical loss coefficient (tan delta)	0.0004–0.0008	0.0004–0.0008
Poisson's ratio	0.29	0.29
Yield strength (elastic limit)	254–819 Mpa	36.9–119 ksi
Fatigue strength at 10^7 cycles	438 Mpa	63.5 ksi
Fracture toughness	120–150 MPa·$m^{1/2}$	109–137 ksi·$in^{1/2}$

Mechanical properties for Co-20Cr-15W-10Ni have been summarized from the following manufacturers specific grades: ASTM F9, Carpenter L-605, Haynes 25, MMPDS L-605, Udimet L-605

Table 4: Chemical composition of Magnesium alloy- WE43 [13]

Element	Content (%)
Yttrium, Y	3.7-4.3
Rare Earths	2.4-4.4
Zirconium, Zr	0.4
Magnesium, Mg	Remainder

The desired properties are assigned to the elements. The 2D property of the element is measured based on the diameter of the strut element. The main branch strut wire diameter is 0.2 mm and the element thickness is 0.05 mm (figure 10) and the side branch strut wire diameter is 0.16 mm and the element thickness is 0.03 mm. The restrains are created in three locations to prevent the rigid body motion of the model. For the stent models 1 and

2, the two ends of the main branch are constrained at the strut bends in the X, Y and Z translations (figure 11). The free end of the side branch is constrained at the strut bends in the X, Y and Z translations. The other end of the side branch is free to expand and has four contact points to prevent the surfaces from expanding one into another.

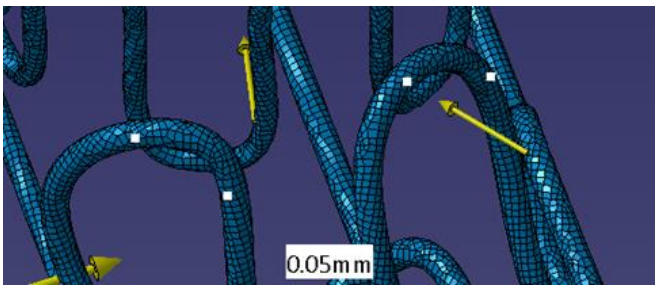

Figure 10: *CATIA model showing the elemental thickness*

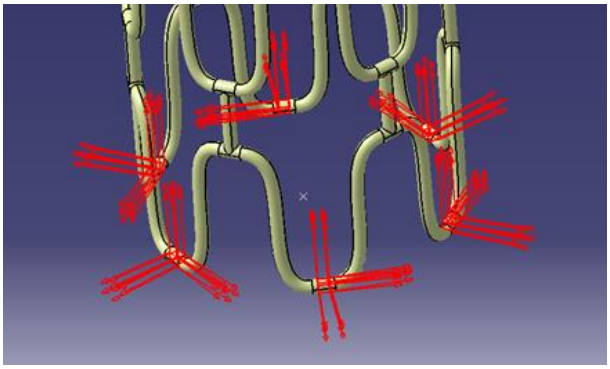

Figure 11: *Boundary Conditions Applied*

The stents are exposed to pulsation loading, balloon inflation pressures are stresses applied by the artery walls. The various loads applied on the stent models are the following. An envelope of the systolic and the diastolic pressures. A patient suffering from a coronary heart disease could experience variations in the blood pressure. A case of hypertension is considered for loading, with a diastolic pressure of 100 mm of Hg and a systolic pressure of 190 mm of Hg. This is equivalent to a diastolic pressure of 0.13 atm and a systolic pressure of 0.25 atm. So, an envelope of 0.25 atm is applied on the stent (figure 13). This also considers the mean arterial pressure of 0.17 atm. within the load envelope.

The mean arterial pressure is calculated by the formula:

$$P_m = P_d + \frac{P_s - P_d}{3}$$

The mean arterial pressure calculation is shown in an illustration in the form of a graph in figure 12.

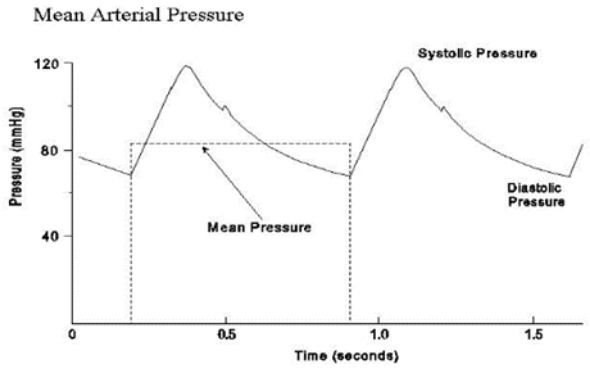

Figure 12: *Illustration of a graphical method of mean arterial pressure calculation [12]*

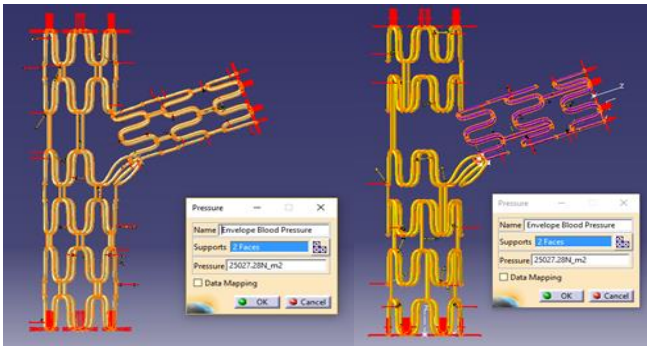

Figure 13: *Application of loads due to blood pressure: models 1, 2*

A radial compression load (figure 14) of 0.5 atm per unit area due to the pre-extension of the artery is applied.

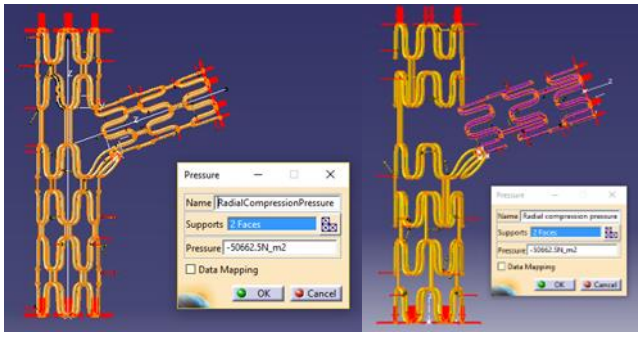

Figure 14: *Application Of Radial Compression Loads On Models 1, 2*

The pulsation loads (figure 15) that are imposed on the stents by contact with the blocked artery vessel walls are also considered and an envelope of 0.25 atm is applied on the stent surfaces.

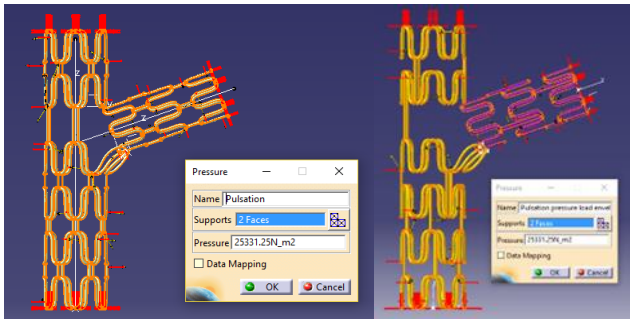

Figure 15: *Application of pulsation load envelope on models 1, 2*

A maximum balloon pressure of 20 atm is considered for the stent designed are balloon expandable stents (figure 16).

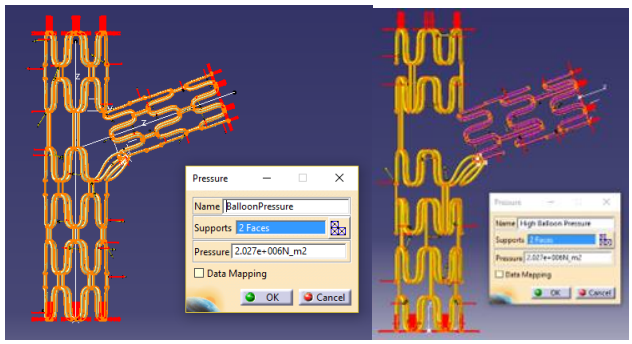

Figure 16: *Application of balloon pressure on models 1, 2*

5. Results And Discussion

Stresses on stent models 1 and 2 were calculated using the loads and boundary conditions mentioned in the above sections.

Peak to Peak Design

Material: 316L SS Annealed

It is seen that the peak to peak design with 316L stainless steel material, when subjected to the loads underwent a maximum displacement of 0.000218 mm which is observed in the carina region (figure 17). The stress distribution in the model shows that the peak to peak design has higher radial strength due to the rings being closer to one another. One design characteristic of the peak to peak design is that the bridge connection will tend to draw adjacent expanding rings away from each other during expansion. This often results in foreshortening, also known as a reduction in length as the stent is expanded.

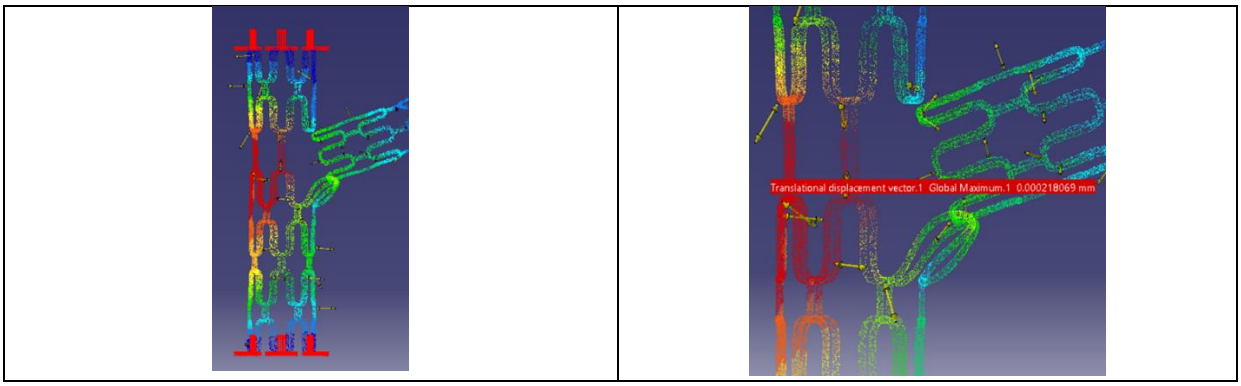

Figure 17: *FE displacement results of model 1 made of 316L SS*

The stresses are maximum in the connection regions between the struts and bridges (figure 18), which is 1.109*107 N/m2.

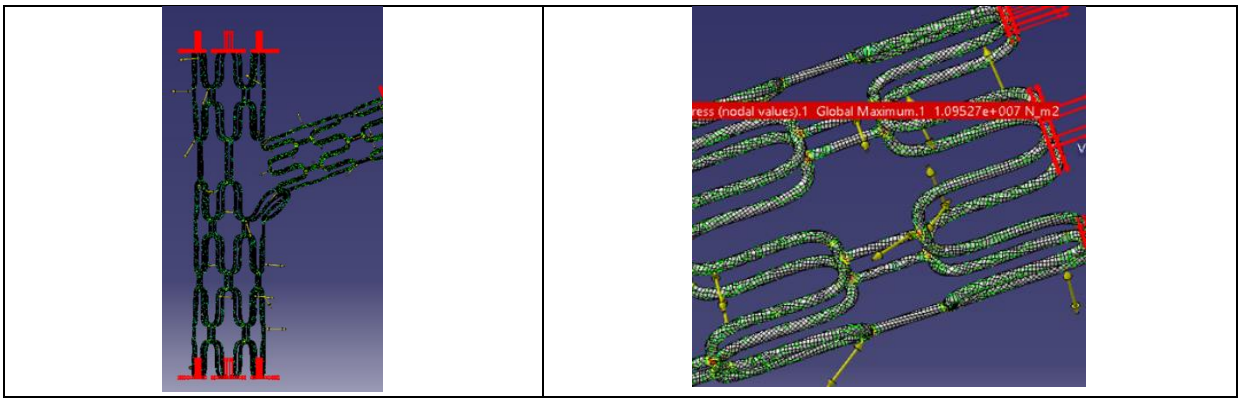

Figure 18: *FE Von Mises stress results of model 1 made of 316L SS*

Material: Cobalt Chromium Alloy- Co-20Cr-15W-10Ni

The peak to peak model for the cobalt chrome alloy underwent a maximum displacement of 0.000175 mm (figure 19), observed in the carina region. The stresses are maximum in the connection regions between the struts and bridges (figure 20), which is 1.103*107 N/m2.

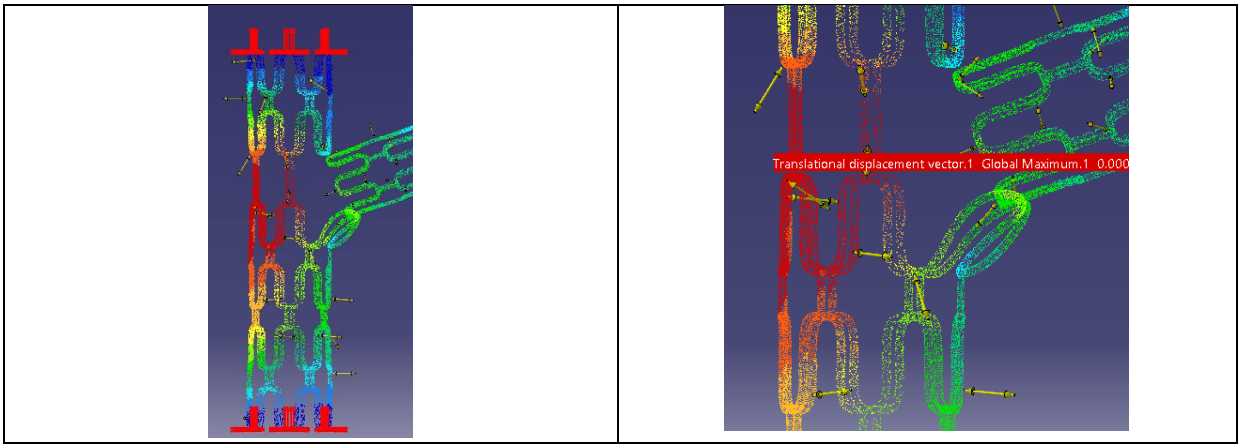

Figure 19: *FE displacement results of model 1 made of cobalt chromium alloy*

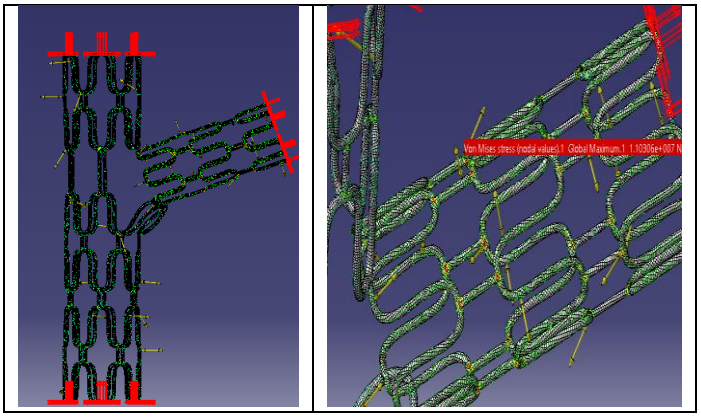

Figure 20: *FE Von Mises stress results of model 1 made of cobalt chromium alloy*

Material: Magnesium alloy WE43: extruded

The peak to peak model for the magnesium alloy, WE43 underwent a maximum displacement of 0.000924 mm, observed in the carina region (figure 21).

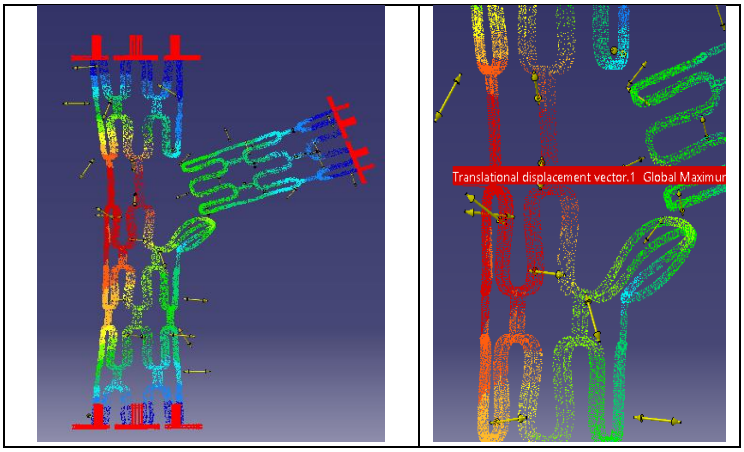

Figure 21: *FE displacement results of model 1 made of magnesium alloy*

It is noticed that the stresses (figure 22) are maximum in the connection regions between the struts and bridges, which is 1.09*107 N/m2.

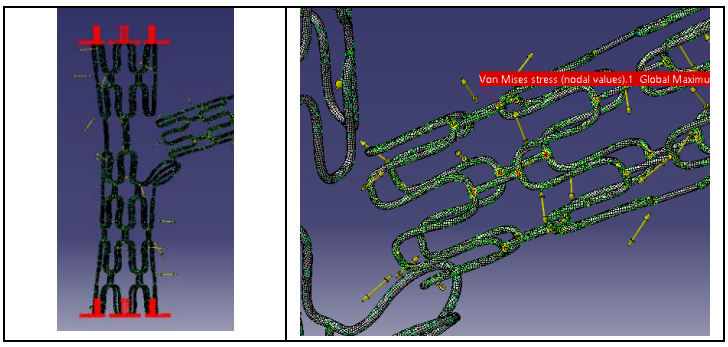

Figure 22: *FE Von Mises stress results of model 1 made of magnesium alloy*

The results of model 1 proves that the bridge connection is tending to draw adjacent expanding rings away from each other during expansion resulting in foreshortening, also known as a reduction in length as the stent is expanded, which is one of the design characteristics of the peak to peak design.

Peak to Valley Design

Material: 316L SS Annealed

It can be seen that the peak to valley design with 316L stainless steel material, when subjected to the loads underwent a maximum displacement of 0.000135 mm which is observed just below the carina region due to the pattern of connectors (figure 23). The stress distribution in the model shows that the peak to valley design has good flexibility with a good radial stiffness compared to peak-to-peak model.

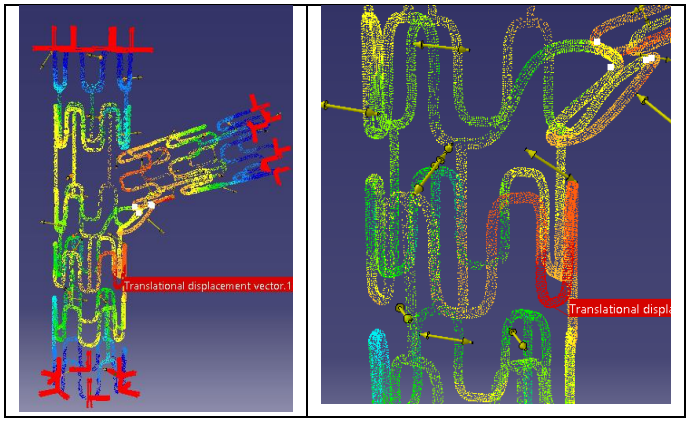

Figure 23: *FE displacement results of model 2 made of 316L SS*

The stresses are maximum in the connection regions between the struts and bridges, which is 1.07x10^7 N/m2 (figure 24).

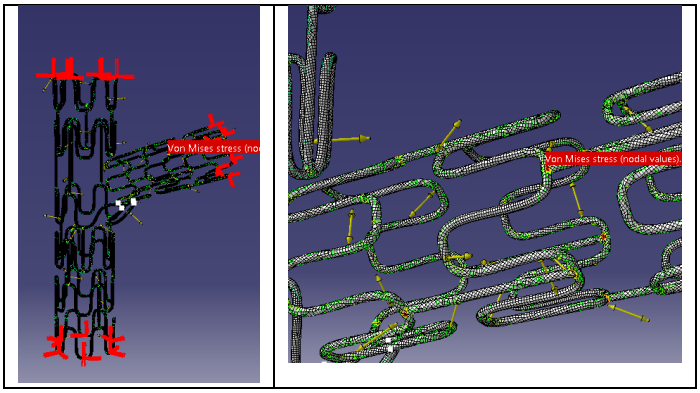

Figure 24*: FE Von Mises stress results of model 2 made of 316L SS*

Material: Cobalt Chromium Alloy- Co-20Cr-15W-10Ni

The peak to valley model for the cobalt chrome alloy underwent a maximum displacement of 0.000113mm, observed in the region just below the carina due to the pattern of connectors (figure 25).

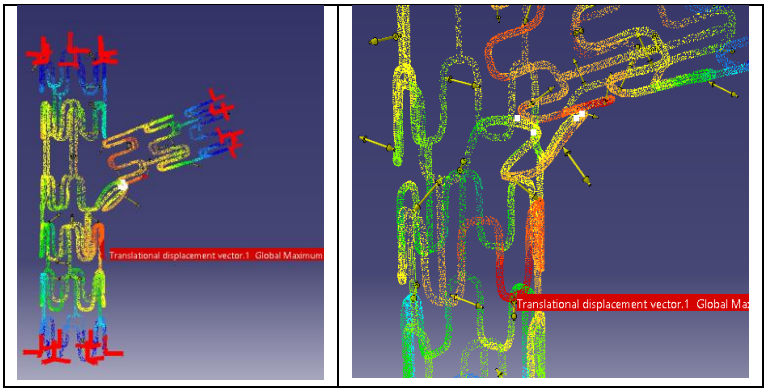

Figure 25: *FE displacement results of model 2 made of cobalt chromium alloy*

The stresses are maximum in the connection regions between the struts and bridges, which is 1.08x10^7 N/m2 (figure 26).

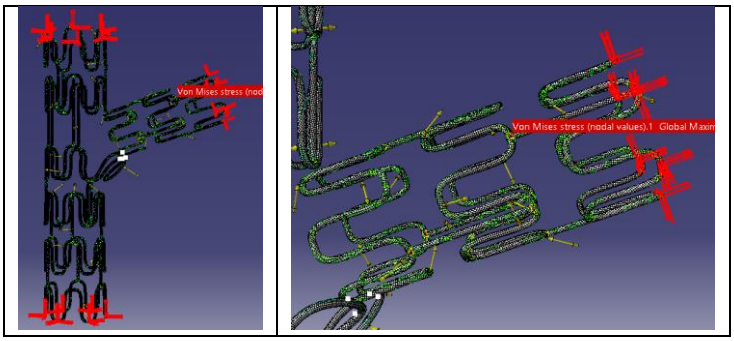

Figure 26: *FE Von Mises stress results of model 2 made of cobalt chromium alloy*

Material: Magnesium alloy WE43 extruded

The peak to valley model for the magnesium alloy, WE43 underwent a maximum displacement of 0.000576 mm, observed in the region just below carina (figure 27). As magnesium is a softer metal, we see few distortions in the struts for this design.

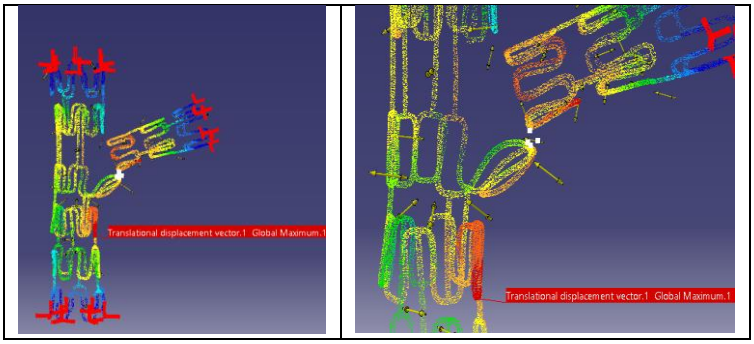

Figure 27: *FE displacement results of model 2 made of magnesium alloy*

The stresses are maximum in the connection regions between the struts and bridges, which is 1.07x10^7 N/m2 (figure 28).

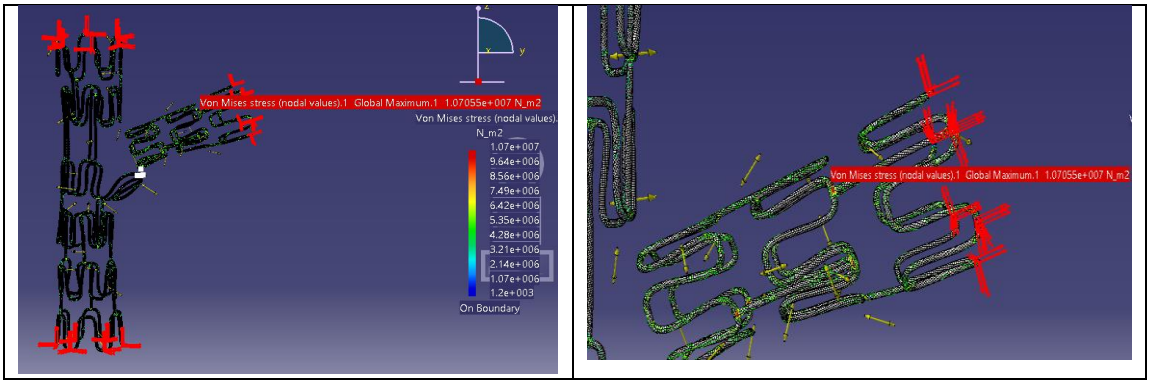

Figure 28: *FE Von Mises stress results of model 2 made of magnesium alloy*

The results of model 2 shows improved scaffolding by eliminating foreshortening and there is better alignment of the struts throughout the stent. However, the connectors or bridges are longer which require extra material.

FE VALIDATION

FE validation is the verification of the model that the behavior of the model to the applied loads and boundary conditions and the analysis conclusions are valid. There are a few parameters in finite element analysis that are uncertain. This accounts for slight differences in the behavior of the real structure and results of the analysis (figure 29).

Model 1

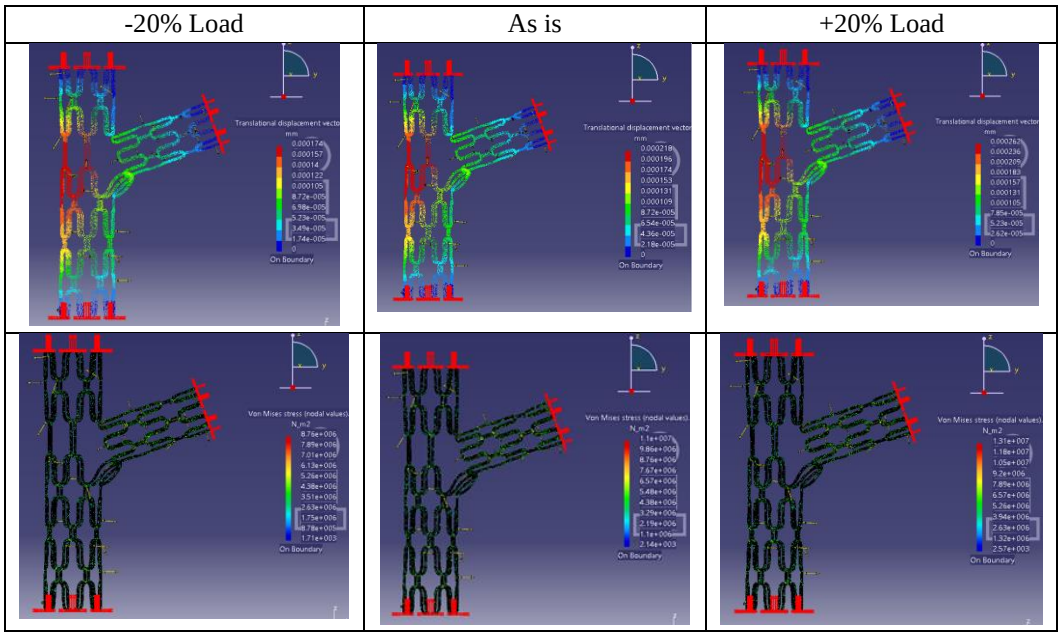

Figure 29: *FE Validation of Model 1*

From table 5, the linear variation of the FE results with the linear variation of the loads when increased by 20% and decreased by 20% proves that there are no singularities or errors in the model.

Table 5: FE Validation of Model 1 (xyz translations constrained)

Material	Yield Strength (N/m^2)	Load	Displacement (mm)	Von Mises (N/m^2)	Factor of Safety
		-20%	0.000174	8.76 E+06	
316L SS, annealed	1.80 E+08	0%	0.000218	1.10 E+07	16.36
		20%	0.000262	1.31 E+07	
Cobalt-Chrome, Co-	2.54 E+08	0%	0.000175	1.10 E+07	23.09

20Cr-15W-10Ni Magnesium alloy, WE43; extruded	1.95 E+08	0%	0.000924	1.10 E+07	17.73

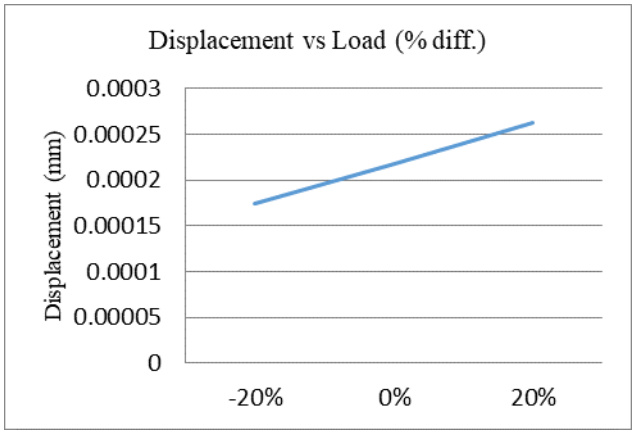

Figure 30: *Graph showing displacement variation with load*

As can be seen in figure 31, the variation of load when increased by 20% and decreased by 20%, the Von Mises stress variation is also linear.

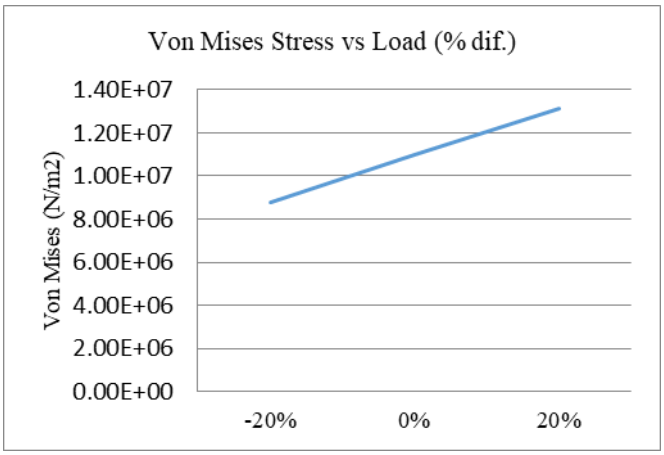

Figure 31: *Graph showing Von Mises Stress variation with load*

Model 2

-20% LOAD	AS IS	+20% LOAD
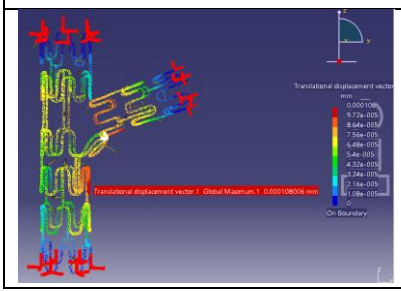	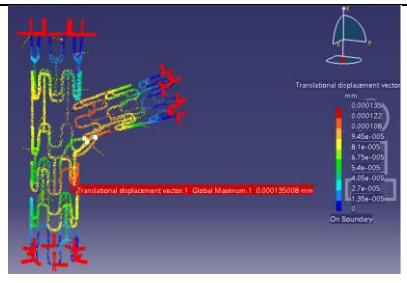	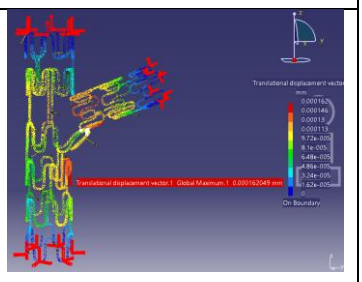

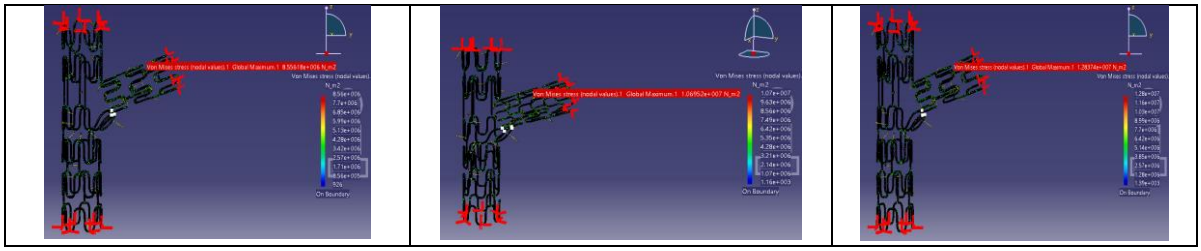

Figure 32: *FE Validation of Model 2*

From table 6, the linear variation of the FE results with the linear variation of the loads when increased by 20 % and decreased by 20 % proves that there are no singularities or errors in the model.

Table 6: FE Validation of Model 2

Material	Yield Strength (N/m2)	Load	Displacement (mm)	Von Mises (N/m2)	Factor of Safety
XYZ Translations Constrained					
316L SS, annealed	1.80 E+08	-20%	0.000108	8.56 E+06	
		0%	0.000135	1.07 E+07	16.82
		20%	0.000162	1.28 E+07	
Cobalt-Chrome, Co-20Cr-15W-10Ni	2.54 E+08	0%	0.000113	1.08 E+07	23.52
Magnesium alloy, WE43; extruded	1.95 E+08	0%	0.000576	1.07 E+07	18.22

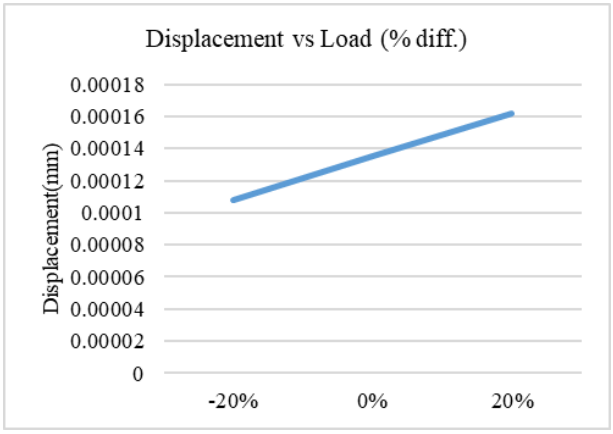

Figure 33: *Graph showing displacement variation with load*

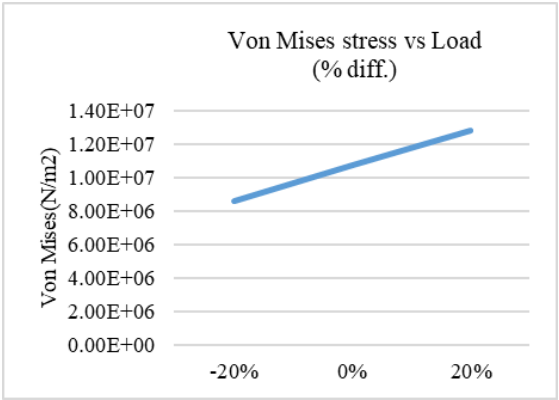

Figure 34: *Graph showing Von Mises Stress variation with load*

The cobalt chrome alloy which is stronger than stainless steel gives us the opportunity of manufacturing thinner struts with the same radial strength. Also, this alloy is denser than stainless steel and hence is more radiopaque which helps monitoring the stent during the placement procedure.

New Design

Design of Model 3

Model 3 is a helical stent design which offers excellent flexibility and resistance to deformation. The body of the stent structure provides good radial strength as well. This stent design has the capability to conform to the tortuous arteries while making way for side branch stenting. This design also has more surface area which aids is a higher amount of medications to be coated (figure 35).

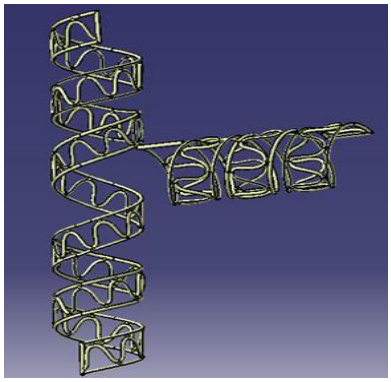

Figure 35: *CATIA Helical model of Bifurcation Stent*

Design Process:

The expanded stent model is modeled in Generative shape modeling. This is parameterized and is dimensionally well controlled. The helixes are modelled in three stages as the region of bifurcation has a different pitch compared to the other stent regions. The struts lie between the two helixes giving it good support. This has a pitch of 4mm for most part of the stent, which could be varied at the bifurcation without deforming. The struts are closed surfaces are converted to a solid in Part Body Design. This is done to be able to clean the model in the end and to extract the surfaces and join them to be able to use for FEA. The position of the side branch is determined and a similar model approach is followed. This model eliminated distortions and there it is not necessary for surface overlaps or contacts. The main and side branch regions close to each other is one end of the side branch and the bottom helix of the main branch. The struts, bridges and helixes solids are joined using Boolean operations. The surfaces of the entire main branch are extracted and joined. The surfaces of the entire side branch are extracted and joined. The ends are filleted to avoid sharp edges.

Finite Element Results for Stent Model 3

For the stent model 3, as the overlap of surfaces has been eliminated, the two ends of the main branch are constrained at the strut ends in the X, Y and Z translations and the two ends of the side branch are constrained at the strut ends in the X, Y and Z translations (figure 36).

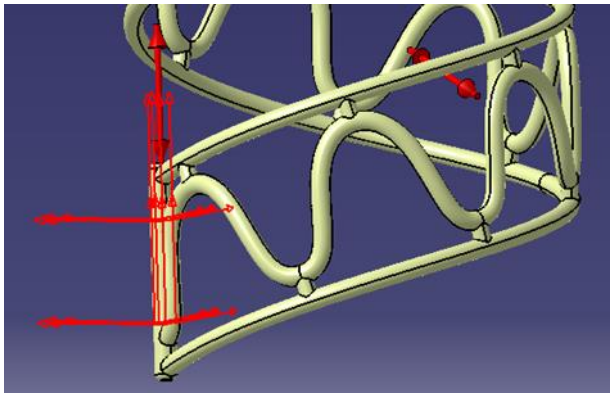

Figure 36: *Boundary Conditions of Helical Model*

Material: 316L SS Annealed

It can be seen that the peak to valley design with 316L stainless steel material, when subjected to the loads underwent a maximum displacement of 0.0000537 mm (figure 37) which is observed in the side branch stent due to the length of the stent. The stress is evenly distributed in the model and shows that the helical design has better flexibility and scaffolding compared to peak-to-peak model and peak to valley stent designs.

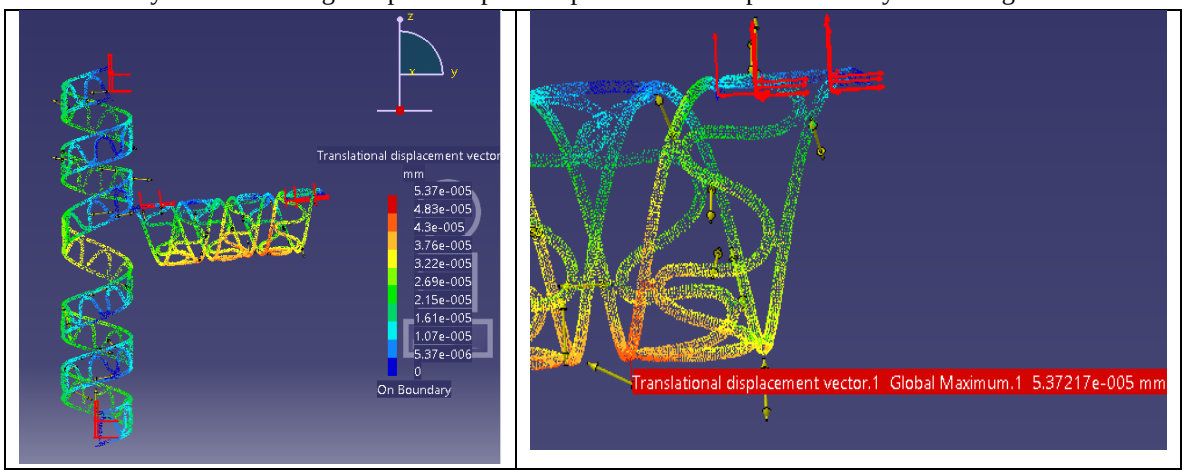

Figure 37: *FE displacement results of helical model made of 316L SS*

The stresses are maximum in the connection regions between the struts and the helix, which is 1.58x107 N/m2 (figure 38).

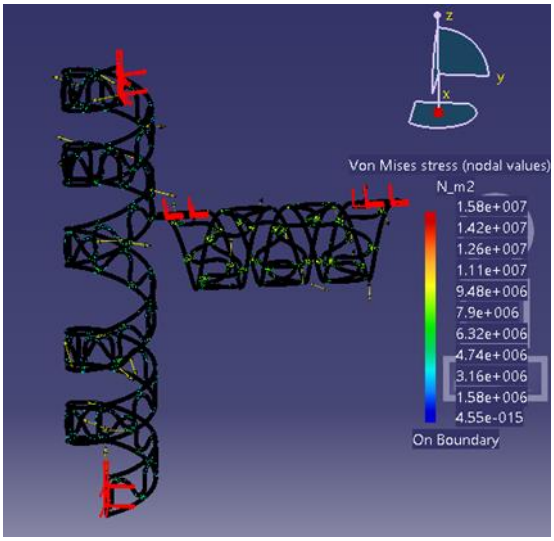

Figure 38: *FE Von Mises stress results of helical model made of 316L SS*

Material: Cobalt Chromium Alloy- Co-20Cr-15W-10Ni

The helical model for the cobalt chrome alloy underwent a maximum displacement of 0.0000433 mm (figure 39), observed in the side branch stent due to the length of the stent.

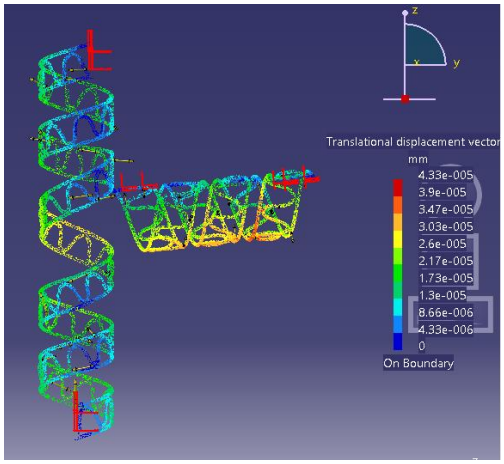

Figure 39: *FE displacement results of helical model made of cobalt chromium alloy*

The stresses are maximum in the connection regions between the struts and the helix (figure 40), which is 1.58x107 N/m2.

Table 7: FE Validation of Helical Model

Material	Yield Strength(N/m2)	Load	Disp. (mm)	von Mises (N/m2)	Factor of Safety
XYZ Translations Constrained					
316L SS, annealed	1.80E+08	-20%	0.0000429	1.26E+07	
		0%	0.0000537	1.58E+07	11.40
		20%	0.0000645	1.90E+07	
Cobalt-Chrome, Co-20Cr-15W-10Ni	2.54E+08	0%	0.0000433	1.58E+07	16.08
Magnesium alloy, WE43; extruded	1.95E+08	0%	0.000228	1.58E+07	12.34

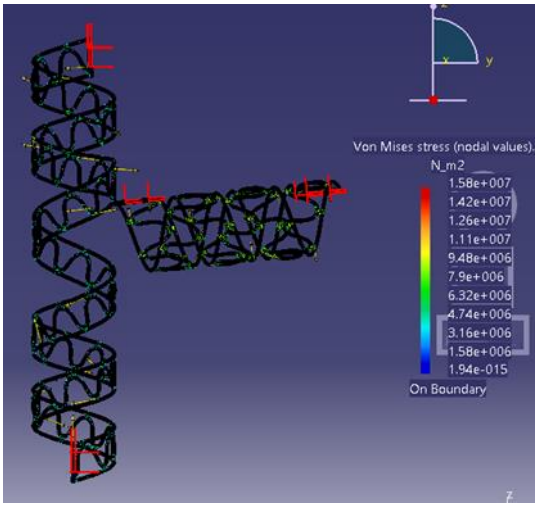

Figure 40: *FE Von Mises stress results of helical model made of cobalt chromium alloy*

Material: Magnesium alloy WE43 extruded

The helical model for the cobalt chrome alloy underwent a maximum displacement of 0.0000433 mm, observed in the side branch stent due to the length of the stent (figure 41).

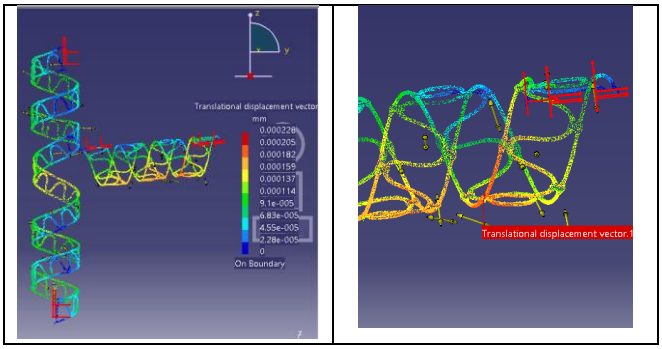

Figure 41: *FE displacement results of helical model made of magnesium alloy*

The stresses are maximum in the connection regions between the struts and the helix, which is 1.58x107 N/m2 (figure 42).

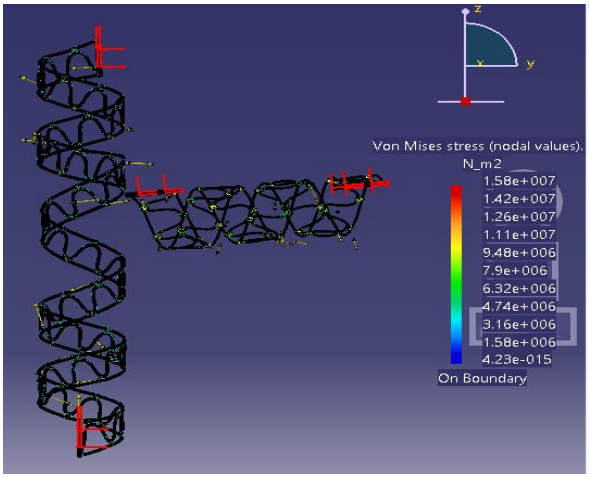

Figure 42: *FE Von Mises stress results of helical model made of magnesium alloy*

FE validation of the helical model

The helical model varies linearly per load variation as can be seen in figure 43.

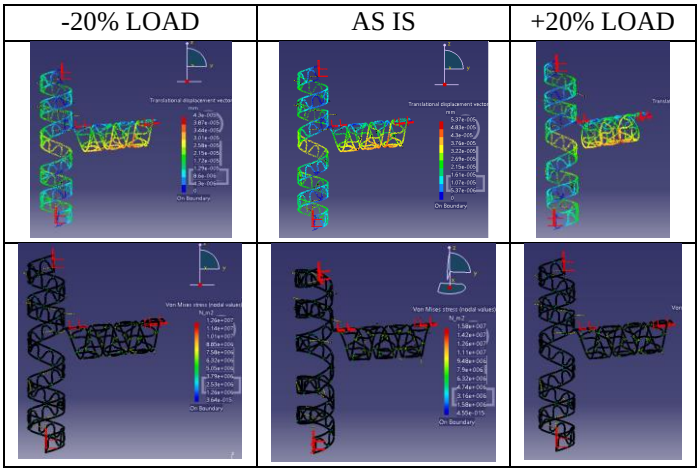

Figure 43: *FE Validation of Helical Model*

From Table 7, the linear variation of the FE results with the linear variation of the loads when increased by 20% and decreased by 20% proves that there are no singularities or errors in the model. The data in figure 44 shows the variation of load when increased by 20% and decreased by 20%, the displacement variation is also linear.

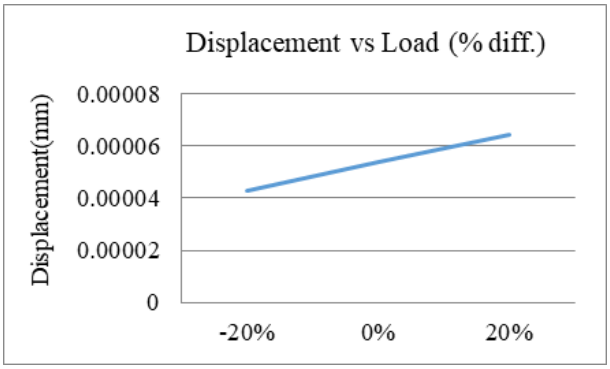

Figure 44: *Graph showing displacement variation with load*

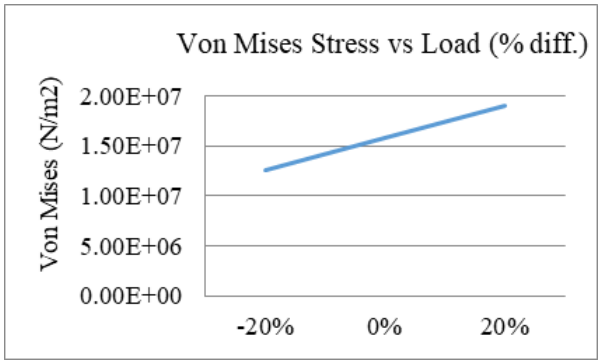

Figure 45: *Graph showing Von Mises Stress variation with load*

Figure 44 shows the variation of load when increased by 20% and decreased by 20%. It depicts a gradual increase from -20% to 20%. The von Mises stress variation versus load increase also shows a similar pattern.

6. Conclusion

Based on the FE results, the helical design performs better when compared to stents with circumferential hoops. It is more flexible than the hoop designs because a helix has an additional degree of flexibility (torsion) with respect to longitudinal bending. The Helical model has a good balance between radial strength and flexibility. This additional degree of freedom results in higher kink resistance and maintains excellent wall apposition under the combined effects of stretching, twisting and bending. According to various studies on helical curvature, it has shown higher survival rate in patients. From a comparison, we see that the displacement in the 316L Stainless Steel helical model is 5.37*10-5 mm which is approximately 2.5 times lesser than the peak to valley model and approximately 4 times lesser than the peak to peak model. This proves that the helical model has better performance as a coronary stent. The maximum Von Mises stress seen in the helical model is in the connections between the struts and the helix which are regions of geometric discontinuities. These regions are stress concentrators also known as stress raisers. The concentration can be reduced by using advanced manufacturing techniques to have filleted edges which aid in smooth stress transfer between the struts and the helix in the stent. Self-expanding stents have some unique advantages. They provide the required flexibility/stiffness during and after the stenting procedure and are unique modalities in metal delivery and must be mastered and many patient will be benefited by it. It has high radial force, it tends to take the shape of the vessel than any other stent, Approximation with lesion is best and the mal-opposition and gap between stent and vessel wall is minimal, hence theoretically there is lower stent thrombosis.

References

[1]. Forensic Medicine for Medical Students, 2010. Retrieved from: http://www.forensicmed.co.uk/

[2]. Wei-Qiang Wang, Dong-Ke Liang, Da-Zhi Yang, Min Qi. (2006) Analysis of the transient expansion behavior and design optimization of coronary stents by finite element method. Journal of Biomechanics, Volume 39, Issue 1, Pages 21-32.
[3]. Stoeckel D., Bonsignore C., Duda S. (2002). A Survey of Stent Designs. Min. Invas. Thermal & Applied Technolgies, 11(4), 137-147.
[4]. Pflederer, Tobias MD; Ludwig, Josef MD; Ropers, Dieter MD; Daniel, Werner G. MD; Achenbach, Stephan MD. (2006). Department of Internal Medicine II (Cardiology), 41(11), 793-798.
[5]. Garasic JM, Edelman ER, Squire JC, Seifert P, Williams MS, Rogers C. Stent and artery geometry determine intimal thickening independent of arterial injury. Circulation 2000;101(7):812–8.
[6]. Justin D Pearlman. Imaging in Coronary Artery Disease, University of California, Los Angeles, David Geffen School of Medicine
[7]. Kastrati A, Mehilli J, Dirschinger J, Dotzer F, Schuhlen H, Neumann FJ, et al. (2001). Intracoronary stenting and angiographic results: strut thickness effect on restenosis outcome (ISAR-STEREO) trial. Circulation 103(23), 2816–21
[8]. Lew M.J. · Angus J.A. (1992). Wall Thickness to Lumen Diameter Ratios of Arteries from SHR and WKY: Comparison of Pressurised and Wire-Mounted Preperations. Journal of Vascular Research, 29, 435-442.
[9]. Ionuţ Gabriel 1, DEVEDŽIĆ Goran, ĆUKOVIĆ Saša. (2015). Parametric Modeling of Surfaces using CATIA v5 Environment, Applied Mechanics and Materials, vol 760. 93-98.
[10]. J. Tambaˇ S. Cani´,D. Paniagua. (2010). A Novel Approach to Modeling Coronary Stents Using a Slender Curved Rod Model: A Comparison Between Fractured Xience-like and Palmaz-like Stents. Applied and numerical partial differential equations. Scientific compuing in simulation, optimization and control in a multidisciplinary context, pg 41-58).
[11]. T. W. Duerig 1 and M. Wholey, S.N. David Chua, B.J. Mac Donald, M.S.J. Hashmi. (2001). A comparison of balloon- and self-expanding stents. Minimally Invasive Therapy & Allied Technologies. 11(4), pp173-178.
[12]. S.N. David Chua, B.J Mac Donald, M.S.J Hashmi. (2002). Finite Element Simulation of Stent Expansion. Journal of Materials Processing Technology. 120. pp 335-340
[13]. D. Mihov, B. Katerska. (2010). Some biocompatible materials used in medical practice Trakia Journal of Sciences, Vol. 8, Suppl. 2, pp 119-125.
[14]. Francesco M., Lorenza P., Maurizio C., Ferdinando A., Riccardo P. (2002). Mechanical behavior of coronary stents investigated through the finite element method. Journal of Biomechanics. 35. pp 803–811.
[15]. Giuseppe S., Gloria M., Pierfrancesco A., Clarissa C., Fabrizio C., Paolo R., Renu V. and Antonio C. (2007). Engineering aspects of stents design and their translation into clinical practice. Ann Ist Super Sanità. | Vol. 43, No. 1. 89-100
[16]. Matthieu De Beule, Peter Mortier, Stephane G. Carlier, Benedict Verhegghe, Rudy Van Impe, Pascal Verdonck, (2007). Realistic finite element-based stent design. Journal of Biomechanics 41, pp 383–389
[17]. Poerner, T. C., Haase, K. K., Wiesinger, B., Wiskirchen, J., & Duda, S. H. (2002). Drug-Coated Stents. Minimally Invasive Therapy and Allied Technologies, 11(4), 185-192.
[18]. Raines, E. W., & Ross, R. (1995). Biology of Atherosclerotic Plaque Formation: Possible Role of Growth Factors in Lesion Development and the Potential Impact of Soy. The Journal of Nutrition, 624S-630S.
[19]. C. Lallya, F. Dolanb, P.J. Prendergasta. (2005). Cardiovascular stent design and vessel stresses: a finite element analysis. Journal of Biomechanics. 38(8), pp 1574-1581.
[20]. Claudio Chiastra, Wei Wu, Benjamin Dickerhoff, Ali Aleiou, Gabriele Dubini, Hiromasa Otake, Francesco Migliavacca, John F. LaDisa. (2016). Computational replication of the patient-specific stenting procedure for coronary artery bifurcations. Journal of Biomechanics. 49(11), pp2102-2111.

[21]. Neil W. Bressloff, Giorgos Ragkousis, and Nick Curzen. (2016). Design Optimization of Coronary Artery Stent Systems. Annals of Biomedical Engineering. 44(2), pp 357-367.
[22]. John F. LaDisa, Jr., Lars E. Olson, Ismail Guler, Douglas A. Hettrick, Said H. Audi, Judy R. Kersten, David C. Warltier, and Paul S. Pagel. (2004). Stent design properties and deployment ratio influence indexes of wall shear stress. Journal of Applied Physiology. 97(1), pp424-430.
[23]. Matthieu De Beule, Peter Mortier, Ste´phane G. Carlier, Benedict Verhegghe, Rudy Van Impe, Pascal Verdonck. (2008). Realistic finite element-based stent design: The impact of balloon folding. Journal of Biomechanics. 41(2), pp383-389.
[24]. Elyasaf Leybovitch, Saar Golan, Moshe Brand. (2015). Mechanical Interaction between Overlapping Stents and Peripheral Arteries - Numerical Model. 2015 IEEE European Modelling Symposium.
[25]. Rebelo, N., Fu, R., & Lawrenchuk, M. (2008). Study of a Nitinol Stent Deployed into Anatomically Accurate Artery Geometry and Subjected to Realistic Service Loading. Journal of Materials Engineering and Performance, 18(5-6), 655-663.
[26]. Ross, R. (1993). The Pathogenesis of Atherosclerosis: A Perspective for the 1990s. Nature, 362, 801-809.
[27]. Ross, R. (1999). Atherosclerosis: An Inflammatory Disease. Mechanisms of Disease, 340(2).
[28]. Runciman, A., Xu, D., Pelton, A. R., & Ritchie, R. O. (2011). An Equivalent Strain/Coffin, amsopm Approach to Multiaxial Fatigue and Life Prediction in Superelastic Nitinol Medical Devices. Biomaterials, 32(22), pp4987-4993.
[29]. Lucas H. Timmins, Michael R. Moreno, Clark A. Meyer, John C. Criscione, Alexander Rachev, James E. Moore Jr. (2007). Stent Artery Biomechanics and Device Design Optimization. Medical & Biological Engineering & Computing. 45(5), pp505-513.